Applied Catalysis B: Environmental 330 (2023) 122619

Contents lists available at ScienceDirect

Applied Catalysis B: Environmental

journal homepage: www.elsevier.com/locate/apcatb

Precise decomplexation of Cr(III)-EDTA and in-situ Cr(III) removal with oxalated zero-valent iron

Minzi Liao [a], Shengxi Zhao [a], Kai Wei [a], Hongwei Sun [a,b,*], Lizhi Zhang [a,b,*]

[a] Key Laboratory of Pesticide & Chemical Biology of Ministry of Education, Institute of Environmental & Applied Chemistry, College of Chemistry, Central China Normal University, Wuhan 430079, PR China

[b] Shanghai Engineering Research Center of Solid Waste Treatment and Resource Recovery, School of Environmental Science and Engineering, Shanghai Jiao Tong University, Shanghai 200240, PR China

ARTICLE INFO

Keywords:
Zero-valent iron
Oxalate
Cr(III) complexes
Singlet oxygen
Decomplexation

ABSTRACT

Cr(III)-organic complexes removal from wastewater is challenging to decompose the complexes without producing toxic Cr(VI). Herein we demonstrated that oxalated zero-valent iron (Ox-ZVI) could one-step decomplex 95.4% of Cr(III)-EDTA with 94.2% removal of total Cr and 60.5% removal of TOC without generating Cr(VI) at pH 6.0. Ox-ZVI with FeC_2O_4 shell preferred to adsorb and activate O_2 to produce more reactive species than ZVI with iron oxide shell, while the generated $^1O_2$ could selectively break the Cr-O and Cr-N bond to precisely decomplex Cr(III)-EDTA without producing Cr(VI). The released Cr(III) was in-situ precipitated on the surface of ZVI in $Cr(OH)_3$ form. Interestingly, •OH preferred the effective degradation of the released EDTA ligand to the oxidation of the chelated Cr(III) at pH 6.0. This study offers a green and facile method for the Cr(III)-organic complexes treatment, and also sheds light on the importance of reactive species adjustment for the precise pollutant control.

1. Introduction

Chromium (Cr)-containing wastewater discharge is of great concern due to its toxicity and the wide application in industries such as tannery, electroplating, etc [1,2]. About 70 million tons of Cr-containing tanning wastewater is discharged annually in China [3]. Therefore, many countries and organizations have strictly regulated the maximum concentration level (MCL) of total Cr besides Cr(VI), e.g., China has stipulated that the MCL of total Cr and Cr(VI) in industrial effluents at 1.5 mg L^{-1} and 0.5 mg L^{-1}, respectively [4]. In wastewater, Cr may exist in forms of free Cr(VI) anion, Cr(III) cation, as well as the Cr(III) complexes due to the ubiquitous natural or anthropogenic ligands such as natural organic matter, EDTA, NTA, citric acid, etc [5,6]. The conventional methods such as adsorption, flocculation and precipitation could effectively remove free Cr ions, but were unsuitable for dealing with Cr(III) complexes of good stability and high solubility. For instance, the alkaline precipitation treatment of a tanning effluent with Cr(III)-carboxyl complexes resulted in ca. 10 mg L^{-1} Cr(III) residual, much higher than the safe level [4].

The safe treatment of Cr(III) complexes generally requires the decomplexation and release of free Cr(III), as well as the prompt removal of Cr(III) and ligands before their recombination. In light of the higher stability constant of Fe complexes, Fe^{3+} is often used to decomplex various metal complexes such as Ni(II), Pb(II), Cu(II), Cd(II), etc. through replacement of central metals [7]. Unfortunately, the displacement of Cr(III) by Fe(III) from complexes was extremely slow because of their comparable stability constants [7]. Recently, advanced oxidation processes (AOPs) have been used to degrade the metal-organic complexes through the oxidative degradation of organic ligands, followed with subsequent adsorption or precipitation of the released metals [8–10]. However, traditional AOPs could not effectively treat Cr (III) complexes, because the highly oxidative species such as •OH might oxidize the central Cr(III) rather than the organic ligands [8,11]. Although the generated Cr(VI) was weakly complexed and would be released from the ligands, its appearance would increase the environmental risks for its much higher toxicity than Cr(III) [11]. Thus, additional reductive species such as Fe(II) was required to reduce Cr(VI) to Cr(III) for subsequent adsorption or precipitation of Cr(III) [11–14]. Moreover, these AOPs based strategies generally required acidic conditions at the decomplexation step to promote the reactive species

* Corresponding authors at: Key Laboratory of Pesticide & Chemical Biology of Ministry of Education, Institute of Environmental & Applied Chemistry, College of Chemistry, Central China Normal University, Wuhan 430079, PR China.

E-mail addresses: sunhw@ccnu.edu.cn (H. Sun), zhanglz@ccnu.edu.cn (L. Zhang).

https://doi.org/10.1016/j.apcatb.2023.122619
Received 27 November 2022; Received in revised form 30 January 2023; Accepted 11 March 2023
Available online 12 March 2023

production for better decomplexation and to prevent the precipitation of iron species [15], but alkaline conditions for the Cr(III) precipitation. Obviously, the inconsistent pH conditions at the two steps would complicate the treatment procedure and increase the cost. Therefore, it is still challenging to one-step remove the Cr(III) complexes without generating Cr(VI) at circumstantial neutral conditions.

Zero-valent iron (ZVI) is widely used in pollutant control because of its outstanding electron donating ability, adsorption capacity, eco-benignancy, and low cost [15–18]. For instance, Fu et al. employed the ZVI-H_2O_2 Fenton oxidation coupled with chemical precipitation to effectively treat the Ni(II)-EDTA containing wastewater [19]. Besides reacting with oxidants, ZVI was able to activate dissolved O_2 at neutral pH to yield various reactive species like $\bullet O_2^-$, H_2O_2, and •OH for the decontamination [20–23], and the Fe^0 core and released Fe(II) of ZVI would inhibit the generation of Cr(VI), while in-situ formed iron oxide during the ZVI corrosion could capture the released Cr(III) via adsorption or precipitation. However, successful removal of Cr(III) complexes only with ZVI is never reported, probably because the easy passivation of ZVI during its fabrication, storage and transportation limits the accessibility of the electrons from Fe^0 core to the iron oxide shell surface [22].

In this work, we demonstrate that oxalated zero-valent iron (Ox-ZVI) prepared via ball milling oxalic acid and ZVI [24,25], could efficiently decomplex Cr(III)-EDTA and remove total Cr and ligands without generating toxic Cr(VI) in one step under the near-neutral condition (pH = 6), because Ox-ZVI could activate molecular oxygen to singlet oxygen ($^1O_2$), which precisely cleaved the Cr-N and Cr-O bonds of Cr(III)-EDTA without oxidizing Cr(III) to Cr(VI), while the released Cr(III) could be in-situ precipitated on the surface of Ox-ZVI in form of $Cr(OH)_3$, thus preventing the re-chelation of Cr(III) and EDTA ligand. Interestingly, •OH produced by the reaction of Ox-ZVI and molecular oxygen did not oxidize Cr(III) under this near-neutral condition, but efficiently degraded the released EDTA ligands. The effective treatment of real tannery wastewater with Ox-ZVI further confirmed the application potential of this one-step strategy.

2. Materials and methods

2.1. Chemicals and reagents

Ethylenediaminetetraacetic acid disodium (Na_2EDTA), chromium trichloride hexahydrate ($CrCl_3$•6 H_2O), oxalic acid dihydrate ($H_2C_2O_4$•2 H_2O), sulfuric acid (H_2SO_4), sodium hydroxide (NaOH) 1,5-diphenylcarbazide, 1,10-phenanthroline (Phen), sodium azide (NaN_3), tertiary butanol (TBA) and ethanol, were obtained from Sinopharm Chemical Reagent. Superoxide dismutase (SOD), commercial ZVI powder (100 mesh, ≥ 99%), 1,5-diphenylcarbazide, tetrabutylammonium bromide, formic acid, sodium formate, acetonitrile, methanol, 2,2,6,6-Tetramethylpiperidine (TEMP), 5,5-dimethyl-1-pyrroline-N-oxide (DMPO), furfuryl alcohol (FFA) and benzoic acid (BA) were purchased from Shanghai Aladdin Biochemical Technology Co., Ltd.

2.2. Preparation of Ox-ZVI

Ox-ZVI was synthesized by planetary ball milling (Boyuntong instrument Technology, Nanjing). 0.18 g oxalic acid dihydrate and 4.0 g of commercial ZVI powder (n($H_2C_2O_4$•2 H_2O): n(Fe) = 2%) were mixed and added with stainless steel milling balls, and sealed in a 100 mL stainless steel jar, which was mounted in the machine and milled at the speed of 500 rpm for 4 h to obtain the Ox-ZVI. The control sample (ZVI) was prepared following the same condition without oxalic acid dihydrate. The preparation protocols of the Ox-ZVI and the ZVI are illustrated by Fig. S1 of Supporting information (SI). The synthesis condition optimizations of Ox-ZVI were provided in Fig. S2-S3, including the molar ratio of oxalate and Fe, ball milling time and ball milling speed. The characterizations of ZVI were provided in Text S1.

2.3. Batch removal of Cr(III)-EDTA

The Cr(III)-EDTA solution was prepared by mixing Na_2EDTA and $CrCl_3$•6 H_2O at the molar ratio of 1:1. The initial concentration of Cr (III)-EDTA was 0.1 mmol L^{-1}, and the pH was adjusted to 6.0 with H_2SO_4 and NaOH aqueous solutions. Batch Cr(III)-EDTA removal experiments were carried out in 250 mL conical flasks open to the air, with 0.4 g of ZVI or Ox-ZVI added to 100 mL of 0.1 mmol L^{-1} Cr(III)-EDTA solution. The flasks were placed in a shaker at 250 rad/min. Then 2 mL of the sample was withdrawn at an interval of 1 h, and filtered through 0.22 μm nylon membrane, for subsequent analysis to determine the concentrations of Cr(III)-EDTA, Cr_{total}, Cr(VI), and TOC. At the end of the reaction, the reacted samples were filtered and vacuum dried for characterization and the Cr(III)-EDTA recycling removal. As for Ar atmosphere control experiments, dissolved oxygen was degassed by Ar bubbling to the air-tight conical flask, which was then connected to an Ar balloon. To explore the main reactive species for Cr(III)-EDTA removal, quenching experiments were carried out with adding1,10-phenanthroline (2 g L^{-1}), SOD (10 mmol L^{-1}), NaN_3 (10 mmol L^{-1}), TBA (1 mL) and ethanol (1 mL) into the Ox-ZVI/Cr(III)-EDTA reaction to scavenge Fe(II), $\bullet O_2^-$, both $^1O_2$ and •OH, •OH, both •OH and Fe(VI), respectively [26,27]. The analytical methods in this study were provided in Text S2.

2.4. Density functional theory (DFT) calculation

The details and methods of DFT calculation were provided in Text S3.

3. Results and discussion

3.1. Cr(III)-EDTA removal performance of ZVI samples

The ZVI and Ox-ZVI samples were first characterized with SEM, TEM, XRD, Mössbauer spectra and XPS (Fig. S5-S9, Table S3-S4, Text S4). The characterization results confirmed that ZVI consisted of α-Fe core and Fe_2O_3 shell, whereas the shell of Ox-ZVI was the mixture of Fe_2O_3 and FeC_2O_4, and more surface Fe(II) existed on Ox-ZVI than ZVI [24], consistent with our previous reports [25]. Subsequently, ZVI and Ox-ZVI were employed to remove Cr(III)-EDTA from a simulated wastewater at near-neutral pH of 6.0 without adding any other oxidants. Within 6 h, ZVI only removed 2.1% of Cr(III)-EDTA and 1.98% of total Cr (Cr_{total}), while Ox-ZVI removed 95.4% of Cr(III)-EDTA and 94.3% of total Cr with the Cr_{total} residual of 5.7 μmol/L (0.3 mg L^{-1}), much lower than the limit of 1.5 mg L^{-1} Cr_{total} regulated by the Integrated Wastewater Discharge Standard of China (GB 8978–1996). More intriguingly, Cr(VI) was not detected during the whole process of Cr(III)-EDTA removal with Ox-ZVI (Fig. 1a). As expected, the TOC concentration of Cr(III)-EDTA solution did not change significantly in case of ZVI, consistent with its negligible Cr(III)-EDTA removal capacity (Fig. S10). In contrast, the addition of Ox-ZVI first increased the TOC from 12.0 to 14.0 mg L^{-1} within the initial 1 h and decreased thereafter, with the final TOC of ca. 5.8 mg L^{-1} at 6 h. This initial increase of TOC may be arisen from the slight release of oxalate from Ox-ZVI (Fig. S11). After subtracting the TOC contribution from released oxalate, the calibrated TOC removal of the Cr(III)-EDTA solution reached ca. 60% after 6 h of Ox-ZVI treatment (Fig. 1b).

To check the contributions of degradation and adsorption to the Cr (III)-EDTA removal, we employed excessive phosphate (10 mmol L^{-1}) to desorb the possibly adsorbed Cr(III)-EDTA from the reacted samples after reaction [28]. This phosphate desorption process increased the Cr (III)-EDTA concentration from 97.9 to 99.7 μmol L^{-1} for ZVI, but from 4.6 to 14.8 μmol L^{-1} for Ox-ZVI (Fig. 1c). The corresponding 1.8 and 10.2 μmol L^{-1} adsorptive removal of Cr(III)-EDTA respectively accounted for 85.7% and 10.7% of total removal of Cr(III)-EDTA for ZVI and Ox-ZVI (Fig. S12), indicating that Cr(III)-EDTA was removed via adsorption for ZVI, but through decomplexation for Ox-ZVI, as verified by the SEM

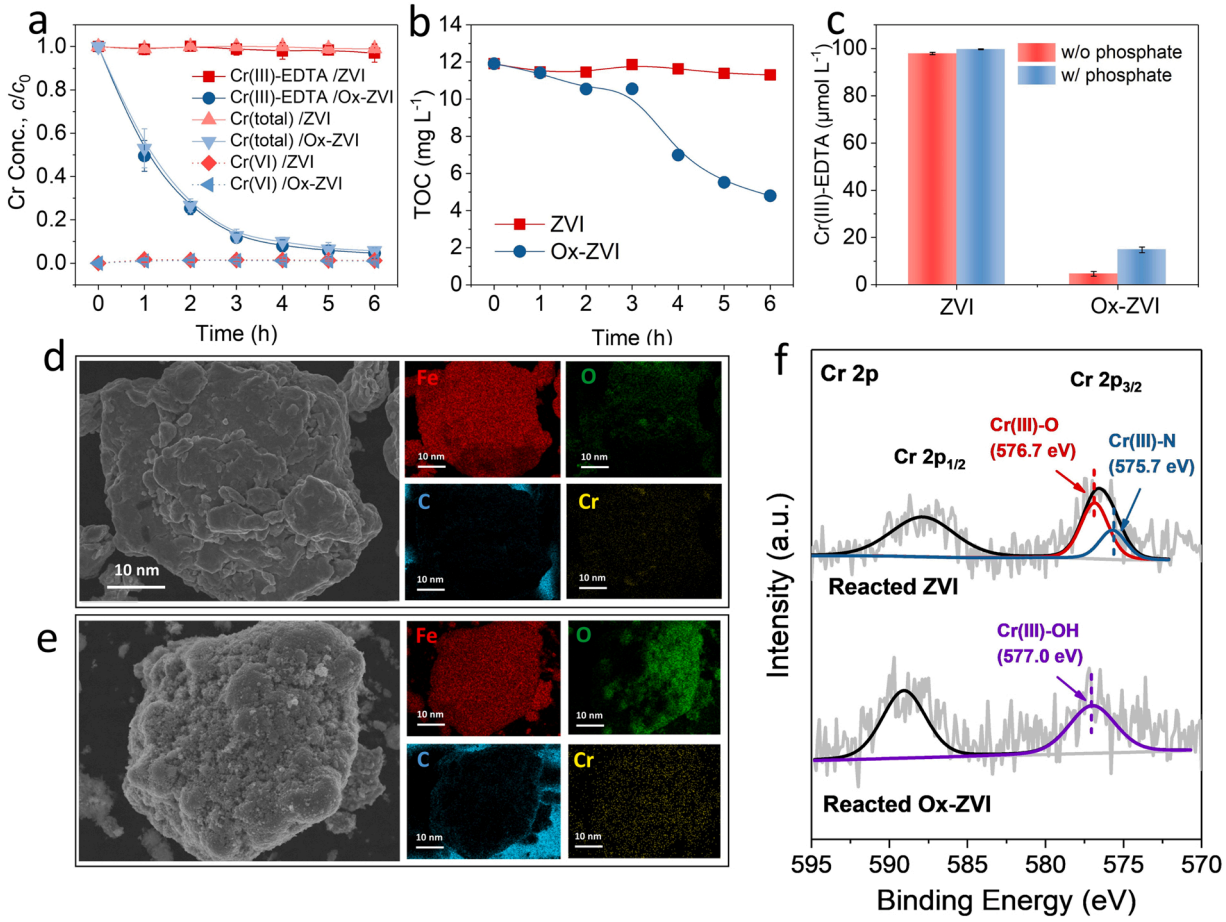

Fig. 1. The time profiles of (a) Cr(III)-EDTA, Cr_{total}, Cr(VI) and (b) TOC removal by ZVI and Ox-ZVI. Note that the TOC contributed by dissolved oxalate in the Ox-ZVI reaction have been subtracted. (c) The influence of phosphate on the concentration of Cr(III)-EDTA in ZVI and Ox-ZVI reactions. The SEM image and the elemental mapping of (d) the reacted ZVI and (e) the reacted Ox-ZVI after Cr(III)-EDTA removal. (f) The Cr 2p HR-XPS spectra of used ZVI and Ox-ZVI. Conditions: $[Cr(III)\text{-}EDTA]_0 = 0.1$ mmol L^{-1}, $[ZVI]_0 = 4.0$ g L^{-1}, $[K_3PO_4]_0 = 10$ mmol L^{-1}, initial pH = 6.0.

and XPS analyses. The SEM and elemental mapping images confirmed that more Cr compounds were deposited on the reacted Ox-ZVI than the reacted ZVI (Fig. 1d and 1e). In the Cr 2p XPS spectra (Fig. 1f), the peaks at 576.7 eV and 575.7 eV appeared for the reacted ZVI, which were attributed to Cr(III)-O and Cr(III)-N. However, these two peaks were not observed for the reacted Ox-ZVI, with the appearance of the Cr(III)-OH signal at 577.0 eV instead. The results showed that Cr existed as Cr (III)-EDTA on the reacted ZVI surface and $Cr(OH)_3$ on the reacted Ox-ZVI surface. So ZVI mainly removed Cr(III)-EDTA by adsorption, while Ox-ZVI could decomplex Cr(III)-EDTA directly and the released Cr^{3+} could hydrolyze to form $Cr(OH)_3$ and deposit on the Ox-ZVI surface.

It is widely accepted that the decomplexation of organic-metal complexes involves the central metal ion replacement and/or ligand oxidation [11,19,29,30], while the corrosion of Fe^0 would release Fe^{2+} and Fe^{3+} in the aqueous solution. We thus monitored the concentration changes of iron ions during the reaction, and found that the maximum concentration of total dissolved iron ions (Fe_{total}) released from ZVI was 8.7 μmol L^{-1} without any detected Fe^{2+}, whereas the maximum concentrations of Fe_{total} and Fe^{2+} released from Ox-ZVI were 25.0 and 18.4 μmol L^{-1}, respectively (Fig. S13). The comparison of complexation stability constants of Fe(II)-EDTA (logK = 14.33), Fe(III)-EDTA (logK = 25.2) and Cr(III)-EDTA (logK = 23.0) suggested that only Fe^{3+} might spontaneously replace the Cr^{3+} of Cr(III)-EDTA [7]. However, the control experiment by mixing 25 μmol L^{-1} Fe^{3+} with Cr(III)-EDTA ruled out this Cr^{3+} replacement because Cr(III)-EDTA did not decrease without generating any Fe(III)-EDTA within 6 h (Fig. S14), might because of the slow kinetics of Fe^{3+}/Cr(III)-EDTA replacement at room temperature [11]. Therefore, we concluded the ligand oxidation might be responsible for the Cr(III)-EDTA removal of Ox-ZVI.

3.2. *Reactive species for Cr(III)-EDTA removal of Ox-ZVI*

We subsequently checked the reactive species responsible for the oxidative Cr(III)-EDTA decomplexation of Ox-ZVI. Regarding that no extra oxidant was introduced during the Ox-ZVI treatment, the reactive species probably stem from the activation of dissolved oxygen [24,25], as confirmed by the strongly suppressed Cr(III)-EDTA removal under Ar atmosphere (Fig. 2a). As O_2 can be reduced to H_2O_2 by Fe^0 in a two-electron transfer pathway (Eq. 1), or to $\bullet O_2^-$ and H_2O_2 by Fe^{2+} in a two-step one-electron transfer pathway (Eqs. 2–3) [22], we added phenanthroline (Phen) to chelate Fe^{2+} and found this chelation significantly inhibited the Cr(III)-EDTA removal of Ox-ZVI with 96.8% of the pseudo-first-order rate constant decreased (Figs. 2b-2c). Meanwhile, the addition of Phen completely halted the H_2O_2 production of Ox-ZVI, but slightly affected the case of ZVI (Fig. S15). These results revealed that ZVI mainly activated O_2 via a two-electron transfer pathway, but the dominant O_2 activation pathway of Ox-ZVI was Fe^{2+} mediated two-step one-electron transfer.

The exact reactive species for the oxidative Cr(III)-EDTA decomplexation of Ox-ZVI was further checked by series of scavenging experiments (TBA to scavenge •OH, EtOH to scavenge both Fe(IV) and •OH, SOD to scavenge $\bullet O_2^-$, NaN_3 to scavenge both $^1O_2$ and •OH). TBA inhibited the Cr(III)-EDTA removal by 35.7%, and the inhibition ratio of

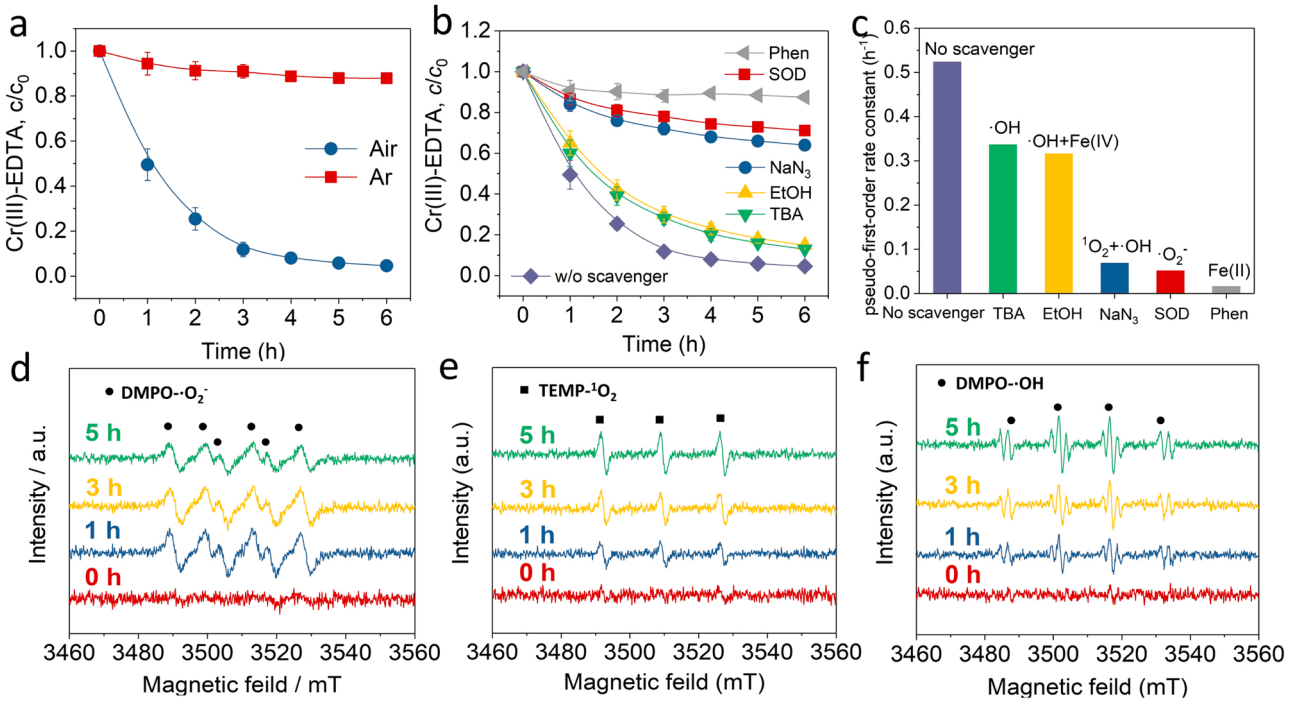

Fig. 2. (a) The impact of different oxygen atmosphere on the Cr(III)-EDTA removal by Ox-ZVI. (b) The Cr(III)-EDTA removal profiles in the Ox-ZVI reaction with different quenching agents. (c) The pseudo-first-order rate constants of Cr(III)-EDTA removal with different scavengers in the Ox-ZVI reaction. The trapped EPR signals of (d) DMPO-•O_2^-, (e) TEMP-$^1O_2$, and (f) DMPO-•OH during the Ox-ZVI reaction. Conditions: $[Cr(III)\text{-}EDTA]_0 = 0.1$ mmol L^{-1}, $[ZVI]_0 = 4.0$ g L^{-1}, $[Phen]_0 = 2.0$ g L^{-1}, $[SOD]_0 = 10$ mmol L^{-1}, $[NaN_3]_0 = 10$ mmol L^{-1}, $[EtOH]_0 = 1\%$ (v/v), $[TBA]_0 = 1\%$ (v/v), initial pH = 6.0.

EtOH was 39.6%, comparable with that of TBA. Therefore, •OH played a considerable role in the Cr(III)-EDTA decomplexation, but the contribution of Fe(IV) could be neglected. Impressively, the inhibition ratios of SOD and NaN_3 respectively were 90.1% and 86.6%, indicating the indispensable roles of •O_2^- and $^1O_2$. The generation of •O_2^-, $^1O_2$ and •OH was further confirmed by the EPR methods with TEMP and DMPO as the trapping agents [31]. The intensity of DMPO-•O_2^- decreased but the intensities of TEMP-$^1O_2$ and DMPO-•OH increased with prolonging the reaction time (Fig. 2d, 2e and 2f), suggesting that •O_2^- might be consumed to produce other two reactive species, as •O_2^- can react with H_2O_2 to produce •OH (the Harbor-Weiss reaction, Eq. 4), and •O_2^- can also transform to $^1O_2$ through its disproportionation (Eq. 5) and oxidation by other stronger oxidants like •OH (Eq. 6) [32,33].

$$O_2 + Fe^0 + 2\,H^+ \rightarrow H_2O_2 + Fe^{2+} \quad (1)$$

$$O_2 + Fe^{2+} \rightarrow \bullet O_2^- + Fe^{3+} \quad (2)$$

$$\bullet O_2^- + Fe^{2+} + 2\,H^+ \rightarrow H_2O_2 + Fe^{3+} \quad (3)$$

$$\bullet O_2^- + H_2O_2 \rightarrow \bullet OH + OH^- + {}^1O_2 \quad (4)$$

$$\bullet O_2^- + \bullet O_2^- + 2\,H^+ \rightarrow H_2O_2 + {}^1O_2 \quad (5)$$

$$\bullet O_2^- + \bullet OH \rightarrow OH^- + {}^1O_2 \quad (6)$$

We thus investigated the kinetics of Cr(III)-EDTA removal to learn the decomplexation mechanism. The reaction rate between Cr(III)-EDTA and reactive species was described as $r = k[Cr(III)\text{-}EDTA][\text{reactive species}]$, which could be approximated to $r = k_{obs}[Cr(III)\text{-}EDTA]$, where $k_{obs} = k[\text{reactive species}]$ (Eqs. 7–9), because of the low and steady concentrations of reactive species. Assuming that the Cr(III)-EDTA degradation by different reactive species were parallel, the apparent rate constant of Cr(III)-EDTA (k_{app}) was the sum of k_{obs} of individual reactive species (Eqs. 10–12). Interestingly, the pseudo-first-order kinetics curve of Cr(III)-EDTA removal by Ox-ZVI could be divided into two stages of 0–3 h and 3–6 h, with k_{app} of 0.708 h^{-1} at the first stage and 0.315 h^{-1} at the second stage, respectively (Fig. 3a). To elucidate the contributions of different reactive species to Cr(III)-EDTA decomplex at the first stage, the Cr(III)-EDTA removal data of the first stage with TBA or NaN_3 were fitted with the pseudo-first order kinetic model. The rate constants were 0.425 h^{-1} with TBA and 0.075 h^{-1} with NaN_3, respectively (Fig. 3a). Then the rate constants of •OH (k^1_{obs}) and $^1O_2$ (k^2_{obs}) were calculated to be 0.283, and 0.350 h^{-1}, accounting for 39.9% and 49.5% of Cr(III)-EDTA removal at the first stage, respectively (Eqs. 10–14). The lower Cr(III)-EDTA removal rate constant of the second stage might be attributed to side reactions such as the competitive consumption of reactive species by degradation intermediates of Cr(III)-EDTA. To confirm this assumption, we conducted reactive species quenching experiments at two stages of Ox-ZVI treatment. NaN_3 inhibited Cr(III)-EDTA removal by 89% and 97% at two stages, respectively (Fig. 3b and 3d), but TBA only inhibited the Cr(III)-EDTA decomplexation by 40% at the first stage, with no significant scavenging effect at the second stage (Fig. 3c and 3d). These results indicated that •OH was severely consumed by the oxidation of the released free ligands, supported by the accelerated removal of TOC at the second stage (Fig. 1b). Thus the decomplexation of Cr(III)-EDTA at the second stage was mainly attributed to $^1O_2$ instead of •OH, highlighting the remarkable reaction selectivity of $^1O_2$ toward Cr(III)-EDTA.

$$Cr(III)\text{-}EDTA + \bullet OH \xrightarrow{k^1} \text{Product } 1k^1_{obs} = k^1[\bullet OH] \quad (7)$$

$$Cr(III)\text{-}EDTA + {}^1O_2 \xrightarrow{k^2} \text{Product } 2k^2_{obs} = k^2[{}^1O_2] \quad (8)$$

$$Cr(III)\text{-}EDTA + \text{other species} \xrightarrow{k^3} \text{Product } 3k^3_{obs} = k^3[\text{other species}] \quad (9)$$

$$k^1_{obs} + k^2_{obs} + k^3_{obs} = k^1_{app} = 0{\cdot}708\ h^{-1} \quad (10)$$

$$k^2_{obs} + k^3_{obs} = k^{TBA}_{app} = 0{\cdot}425\ h^{-1} \quad (11)$$

$$k^3_{obs} = k^{NaN3}_{app} = 0{\cdot}075\ h^{-1} \quad (12)$$

$$\text{Contribution of } \bullet OH = k^1_{obs} / k^1_{app} \quad (13)$$

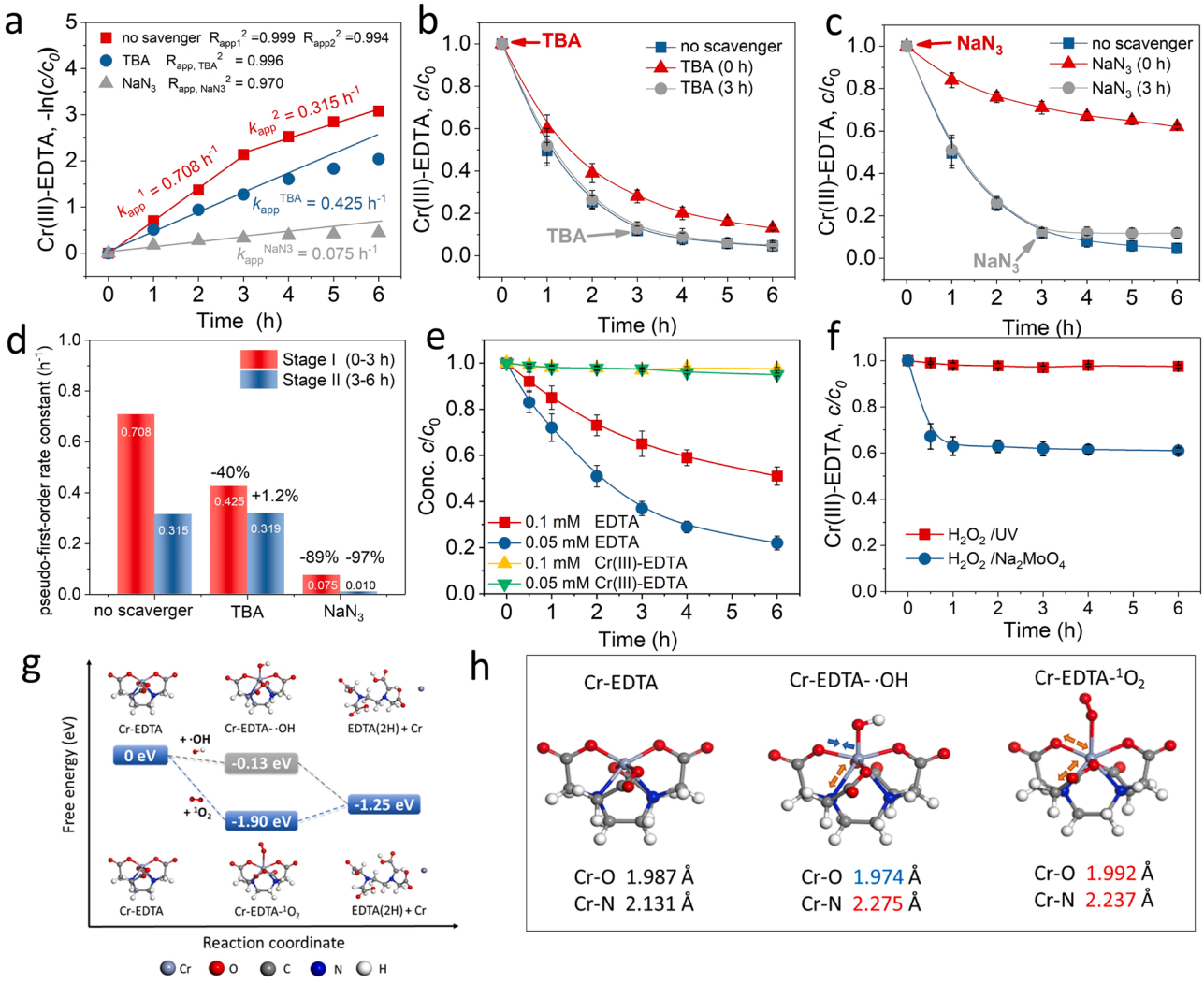

Fig. 3. (a) The pseudo-first-order kinetic model fitted Cr(III)-EDTA removal curves in the Ox-ZVI reactions. The impact of (b) NaN_3 and (c) TBA added at different time on the Cr(III)-EDTA removal profile by Ox-ZVI. (d) The pseudo-first-order rate constants of two stages in (b) and (c) reactions. (e) The removal of Cr(III)-EDTA and EDTA by the H_2O_2/UV reaction·$[H_2O_2]_0$ = 0.5 mM, λ_{UV} = 365 nm, intensity = 0.8 mW/cm^3. (f) The Cr(III)-EDTA removal by the (0.5 mM) H_2O_2/UV and the (2.0 mM) H_2O_2/Na_2MoO_4 reactions. (g) The energy profiles of the Cr(III)-EDTA decomplexation process induced by $^1O_2$ or •OH. (h) The change of coordinating bond length of the Cr(III)-EDTA with $^1O_2$ or •OH. Conditions: $[Cr(III)\text{-}EDTA]_0$ = 0.1 mmol L^{-1}, $[ZVI]_0$ = 4.0 g L^{-1}, $[NaN_3]_0$ = 10 mmol L^{-1}, $[TBA]_0$ = 1% (v/v), initial pH = 6.0.

Contribution of $^1O_2 = k_{obs}^2 / k_{app}^1$ (14)

To clarify the contributions of $^1O_2$ and •OH to the decomposition of Cr(III)-EDTA, we quantified the steady-state concentrations of $^1O_2$ and •OH ($[^1O_2]_{ss}$ and $[•OH]_{ss}$) during the Ox-ZVI treatment using BA and FFA as probes according to the previously reported methods (Text S1) [32,34–36]. As shown in Fig. S16, $[•OH]_{ss}$ produced by Ox-ZVI was 6.5 × 10^{-15} mol/L, 2 orders of magnitude lower than $[^1O_2]_{ss}$ (4.8 ×10^{-13} mol/L). To further distinguish the roles of $^1O_2$ and •OH in Cr(III)-EDTA decomplexation, we carried out control experiments to remove Cr (III)-EDTA with H_2O_2/UV and H_2O_2/Na_2MoO_4 reactions, which were reported to produce •OH or $^1O_2$, respectively (Eq. 15-16) [33,37,38]. For better comparison, we first optimized the parameters of the control experiments to achieve the comparable concentrations of reactive species with the Ox-ZVI system at the initial pH of 6.0 (Fig. S17), with H_2O_2/UV ($[H_2O_2]$ = 0.5 mM, UV 365 nm intensity = 0.8 mW/cm^3) and H_2O_2/Na_2MoO_4 ($[H_2O_2]$ = 2 mM, $[Na_2MoO_4]$ = 4 mM) employed for the next experiments, where H_2O_2 could not degrade Cr(III)-EDTA (Fig. S18a). Surprisingly, H_2O_2/UV of $[H_2O_2]$ = 0.5 mM could not decomplex Cr(III)-EDTA, but degrade EDTA efficiently (Fig. 3e), although significant Cr(III)-EDTA decomplexation was achieved with H_2O_2/UV of $[H_2O_2]$ higher than 5.0 mM (Fig. S18b). In contrast, the H_2O_2/Na_2MoO_4 counterpart could effectively decomplex Cr(III)-EDTA (Fig. 3 f and Fig. S18c). Obviously, these results were different from previous reports of Cr(III)-EDTA decomplexation with •OH under acidic pH [11–13], which was reasonable because pH was between 6 and 7 during the whole Cr(III)-EDTA removal with both Ox-ZVI and ZVI (Fig. S19), while both the yield and oxidizing ability of •OH would significantly weaken under neutral conditions, resulting in the much poorer performance of •OH to oxidize Cr(III)-EDTA, consistent with some previous results [7,33]. Therefore, we conclude that $^1O_2$ is the major reactive species to decomplex Cr(III)-EDTA during the Ox-ZVI treatment, and the contribution of •OH at the first stage might stem from the production of $^1O_2$ by •OH through Eq. 6, which is thermodynamically spontaneous with ΔG = − 1.31 eV (−127 kJ mol^{-1}) at pH 7 [33]. Whereas after 3 h, EDTA released by Cr(III)-EDTA consumed plenty of •OH to suppress the $^1O_2$ production, thus slowing the Cr (III)-EDTA removal at the second stage.

$H_2O_2 \xrightarrow{h\nu} 2 \bullet OH$ (15)

$$2H_2O_2 \xrightarrow{Na_2MoO_4} {}^1O_2 + 2O \quad (16)$$

DFT calculation was further employed to understand the different reactivities of $^1O_2$ and •OH for Cr(III)-EDTA decomposition. At pH 6–7, Cr(III)-EDTA existed in form of Cr(III)-EDTA$^-$, and EDTA was in form of EDTA(H)$^{3-}$ (Fig. S20) [39]. The change of energy (ΔE) to form the transition state of Cr(III)-EDTA$^-$-$^1O_2$ was − 1.90 eV, significantly lower than that (−0.13 eV) of Cr(III)-EDTA$^-$-•OH (Fig. 3 g), confirming that $^1O_2$ was more prone to attack Cr(III)-EDTA than •OH. Then the ΔE of Cr (III)-EDTA$^-$ oxidation to generate EDTA(2 H)$^{2-}$ and Cr atom was − 1.12 eV and + 0.65 eV for •OH and $^1O_2$, respectively. Both absolute values of ΔE were less than 1.5 eV, validating that both reactions could proceed spontaneously at room temperature [40]. Meanwhile, the binding of •OH elongated the length of Cr-N bond in Cr(III)-EDTA from 2.131 Å to 2.275 Å, but shortened its Cr-O length from 1.987 Å to 1.974 Å. On the contrary, both the Cr-O and Cr-N bonds were elongated after binding to $^1O_2$ (Cr-O 1.992 Å and Cr-N 2.237 Å) (Fig. 3 h). Due to the strong oxidation ability of •OH, all the electrons of Cr, O and N atoms would be taken by •OH, enlarging the charge difference between Cr-O (from 0.69 to 0.705) and Cr-N (from 0.48 to 0.515) (Fig. S21 and Table S3). Thus, the attraction between atoms increased, and the bond length would be shortened. However, $^1O_2$ of weak oxidation ability would mainly capture the electrons of the coordination O to decrease the charge difference between Cr-O (from 0.69 to 0.6625) and Cr-N (from 0.48 and 0.47) (Table S3). This weakened interatomic attraction would elongate the bond length, making the Cr-O and Cr-N bonds unstable for further destruction. Thus, $^1O_2$ was more effective to decomplex Cr (III)-EDTA. Regarding that the oxidation capacity of $^1O_2$ is lower than that of Cr(VI) ($E^{\Theta}(^1O_2/\bullet O_2^-) = 0.81$ V < $E^{\Theta}(Cr_2O_7^{2-}/Cr^{3+}) = 1.232$ V), it was hard for $^1O_2$ to oxide Cr(III) to Cr(VI). Thus, $^1O_2$ could realize the Cr (III)-EDTA decomplexation without generating more toxic Cr(VI), offering a green decomplexation pathway.

We also utilized LC-MS to monitor the intermediates for clarifying the degradation pathways of Cr(III)-EDTA during the Ox-ZVI treatment (Fig. 4). EDTA(2 H)$^{2-}$ and ethylenediamine-N, N'-diacetic acid (ED2A (2 H)) were detected, whereas the common degradation intermediates of ligand oxidizing decomplexation such as Cr(III)-ED3A and Cr(III)-ED2A were not found, revealing that the attack site of $^1O_2$ was the central Cr atom rather than the ligand groups to achieve the precise decomplexation of Cr(III)-EDTA. These LC-MS results were consistent with the DFT calculation results. Then, the released ligand EDTA(2 H)$^{2-}$ was gradually oxidized to ED3A and ED2A by •OH and $^1O_2$, and finally mineralized to CO_2 and H_2O. The free Cr^{3+} ion could be hydrolyzed to Cr $(OH)_3$ and deposited on Ox-ZVI surface, as supported by the XPS result (Fig. 1f). Acid dissolution experiments of reacted ZVI and Ox-ZVI also demonstrated precipitation of Cr on Ox-ZVI surface in form of Cr(III) (Fig. S22).

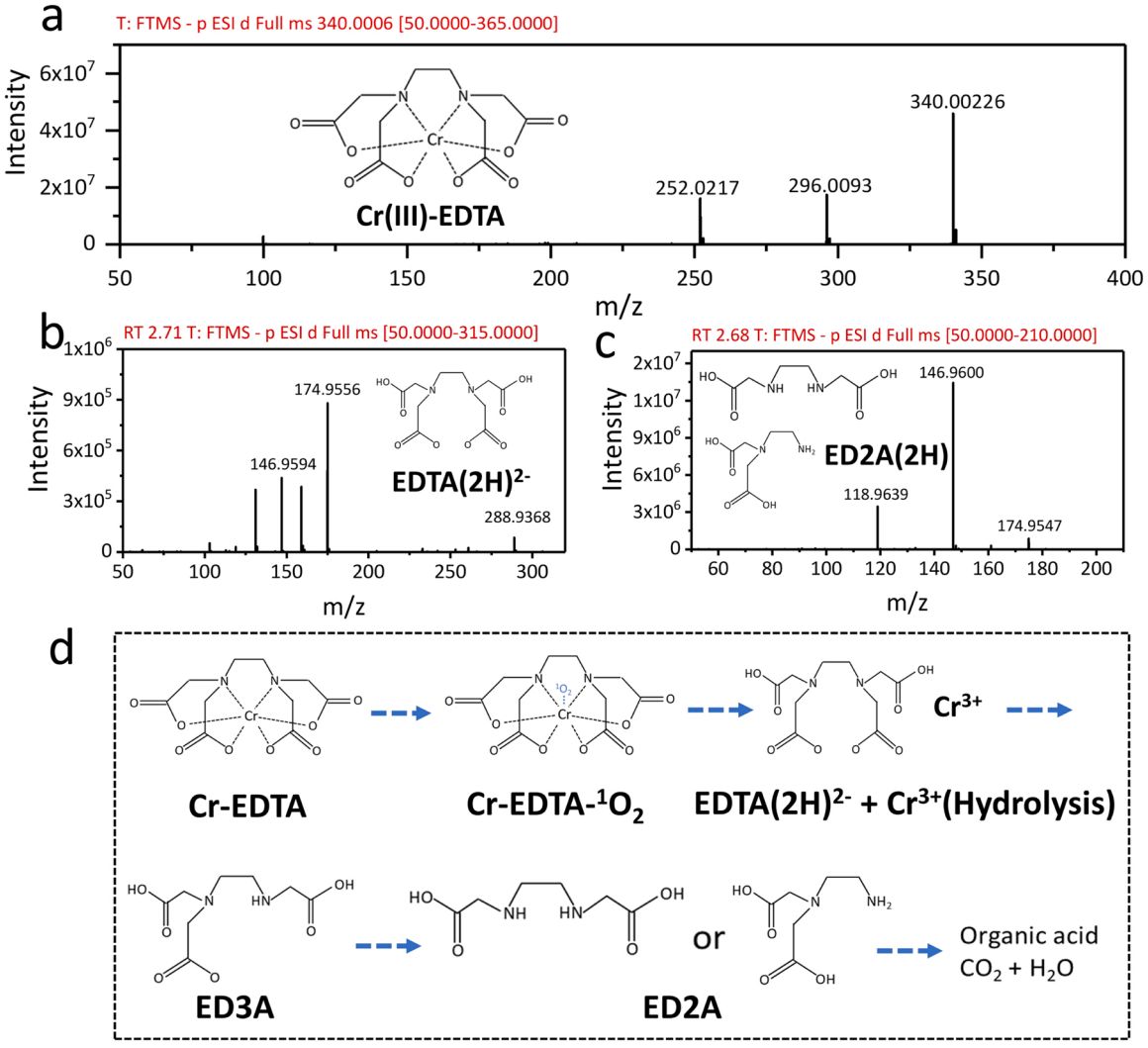

Fig. 4. The LC-MS spectra of (a) the Cr(III)-EDTA, (b) the EDTA(2 H)$^{2-}$ intermediate, and (c) the ED2A(2 H) intermediate detected during the Cr(III)-EDTA degradation by Ox-ZVI^s. (d) The possible decomplex and degrading pathways of Cr(III)-EDTA in the Ox-ZVI reaction.

3.3. Enhanced reactive species production of Ox-ZVI

To understand the enhanced production of reactive species by Ox-ZVI via molecular oxygen activation, we first monitored the concentrations of dissolved oxygen during the Cr(III)-EDTA decomplexation. As expected, the Ox-ZVI consumed more dissolved oxygen than ZVI during the reaction (Fig. 5a). Regarding that ZVI and Ox-ZVI are respectively covered by the Fe_2O_3 shell and the mixture of Fe_2O_3 and FeC_2O_4, while the oxygen activation of molecular oxygen is determined by its adsorption on the surface of the ZVI, we theoretically investigated the O_2 adsorption on the surface of Fe_2O_3 and FeC_2O_4 with DFT calculation (Fig. 5b and 5c). The adsorption energies of O_2 on Fe_2O_3 and FeC_2O_4 was − 2.45 and − 2.80 eV, indicative of more favorable adsorption of O_2 on the Ox-ZVI surface. Moreover, the charge (−0.29) of O_2 on the FeC_2O_4 surface was more negative than that (−0.08) on the Fe_2O_3 surface, indicating that the adsorbed O_2 was more likely to get electrons from the FeC_2O_4 surface than from Fe_2O_3. This stronger O_2 electron withdrawing effect of the FeC_2O_4 surface would facilitate the electron transfer from Fe^0 core to FeC_2O_4 shell and subsequently to the adsorbed O_2, thus promoted the reduction of O_2 on the surface of Ox-ZVI. As Fe_2O_3 and FeC_2O_4 only removed 3.2% and 5.4% of Cr(III)-EDTA within 6 h, respectively (Fig. 5d), the effective activation of O_2 required the electron from the Fe^0 core of ZVI to the surface. Subsequently, the electron donating capacities of the two ZVI samples were characterized with electrochemical methods. The Tafel scanning results showcased that the corrosion potential of Ox-ZVI (−0.58 V) was more negative than that (−0.49 V) of ZVI, and the corrosion current of Ox-ZVI (log(i/A) = −4.8) was higher than that (log(i/A) = −5.0) of ZVI (Fig. 5e), confirming that Ox-ZVI possessed stronger electron donating capacity than ZVI, which was also consistent with the lower impedance of Ox-ZVI than that of ZVI (Fig. 5f). All these results revealed that Ox-ZVI could more efficiently adsorb molecular oxygen and donate electrons for molecular oxygen activation. The electron selectivity of Ox-ZVI (Text S5) was also discussed. The electron selectivity of ZVI and Ox-ZVI for O_2 activation were 1.3% and 4.0% after calculation (Fig. S23), indicating that the electron selectivity of Ox-ZVI was improved.

Ox-ZVI exhibited excellent Cr(III)-EDTA removal efficiency even after 5 cycles, with 85% Cr(III)-EDTA and 79% total Cr removal without producing Cr (VI), as well as the residual Cr_{total} (1.09 mg L^{-1}) lower than the standard of GB 8978–1996 (Fig. 5g). For a real tanning wastewater with 25 mg L^{-1} Cr_{total} and 5.5 mg L^{-1} free Cr (VI), 8 h of Ox-ZVI treatment respectively reduced the concentrations of Cr_{total} and Cr(VI) to 1.4 and 0.43 mg L^{-1}, with 94.4% of Cr_{total} and 92.2% of Cr(VI) removal efficiencies, realizing the standard discharge according to GB

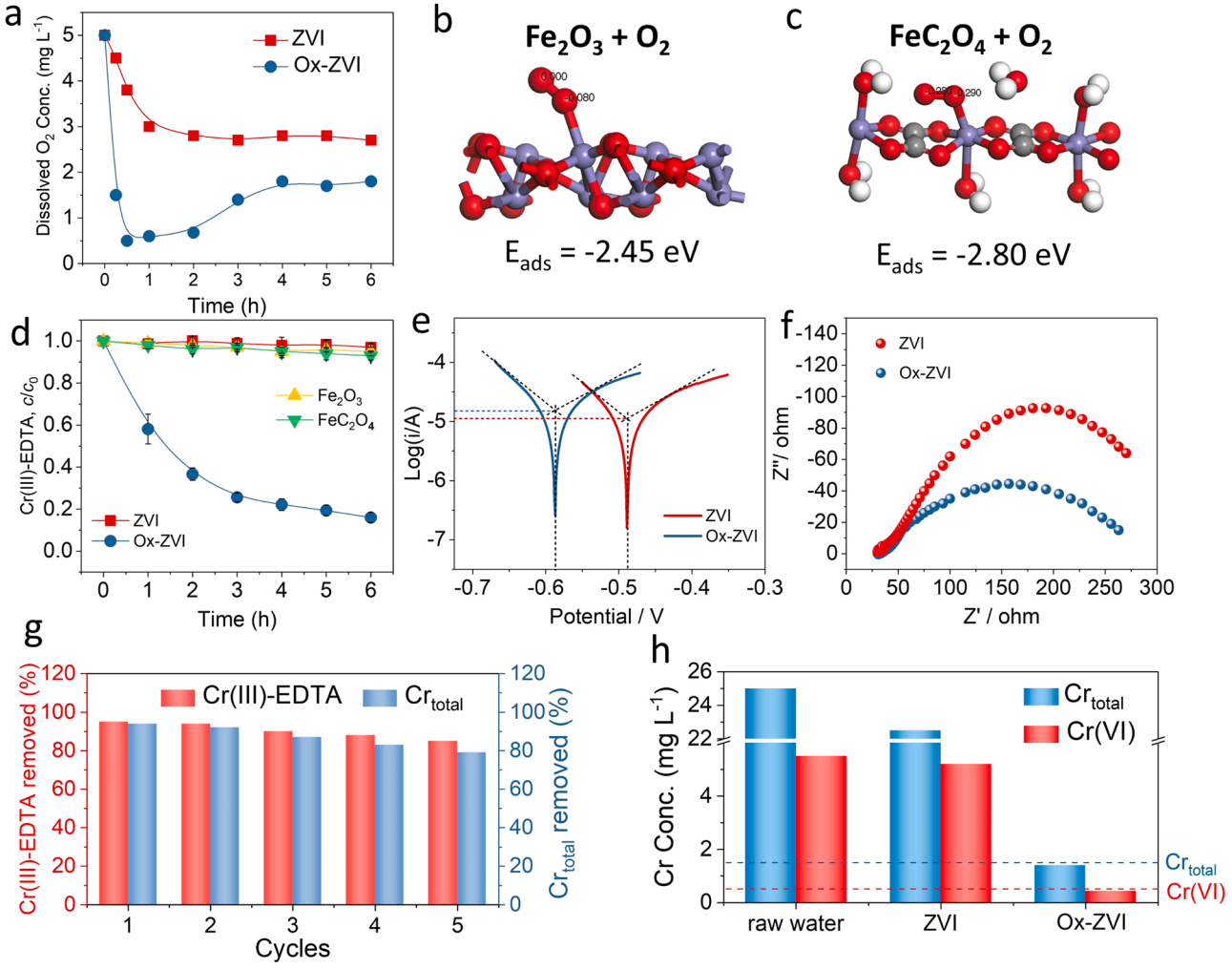

Fig. 5. (a) The concentrations of dissolved oxygen during the Cr(III)-EDTA removal processes by ZVI and Ox-ZVI. (b-c) The adsorption model and the adsorption energy of O_2 on Fe_2O_3 and FeC_2O_4, respectively. (d) The Cr(III)-EDTA removal performance of the Fe_2O_3 and FeC_2O_4 controls. (e) Tafel scans and (f) Nyquist plots of ZVI and Ox-ZVI. Conditions: $[Cr(III)\text{-}EDTA]_0$ = 0.1 mmol L^{-1}, $[ZVI]_0$ = 4.0 g L^{-1}, $[Fe_2O_3]_0 = [FeC_2O_4]_0$ = 71.1 mmol L^{-1}, initial pH = 6.0 (g) The reusability of Ox-ZVI to remove Cr(III)-EDTA and Cr_{total} from the simulated wastewater. Conditions: $[Cr(III)\text{-}EDTA]_0$ = 0.1 mmol L^{-1}, $[Ox\text{-}ZVI]_0$ = 4.0 g L^{-1}, initial pH = 6. (h) The performances of ZVI and Ox-ZVI to remove Cr_{total} and Cr(VI) from a real tanning wastewater sample obtained from Sichuan Province, China. Conditions: $[ZVI]_0 = [Ox\text{-}ZVI]_0$ = 8 g L^{-1}, initial pH = 6.0.

8978–1996 (Fig. 5h).

4. Conclusion

In this study, we demonstrated that Ox-ZVI could one-step decomplex Cr(III)-EDTA to remove total Cr and TOC without generating toxic Cr(VI) at pH 6.0. Ox-ZVI with ferrous oxalate shell was beneficial for the adsorption and activation of O_2 to produce more reactive species than the ZVI counterpart with iron oxide shell. The generated $^1O_2$ by Ox-ZVI/O_2 could selectively break the Cr-O and Cr-N bonds to precisely decomplex Cr(III)-EDTA without producing Cr(VI), with the released Cr (III) in-situ precipitated on the surface of Ox-ZVI in form of $Cr(OH)_3$. Interestingly, the generated •OH preferred the effective degradation of the released EDTA ligand to the oxidation of the chelated Cr(III) under the near neutral condition. This work offers a green and convenient method to handle with the complexed Cr(III) wastewater by simply mixing the Ox-ZVI aerobically under circumstantial pH, avoiding the problems encountered by traditional AOPs such as the production of toxic Cr(VI), the reduction need of Cr(VI), the inconsistent pH for decomplexation and Cr(III) precipitation. Therefore, the reduced cost and simplified wastewater treatment procedures can be expected. This work also sheds light on the importance of reactive species adjustment for the precise pollutant control. Nevertheless, the electron selectivity of Ox-ZVI to activate molecular oxygen is still low (ca. 4%) in this work, thus more effort should be made in the future to improve the effective utilization of ZVI electrons for better oxygen reduction efficiency.

CRediT authorship contribution statement

Minzi Liao: Investigation, Data curation, Conceptualization, Methodology, Writing – original draft. **Shengxi Zhao**: Methodology, Software. **Kai Wei**: Data curation, Methodology. **Hongwei Sun**: Funding acquisition, Investigation, Writing – review & editing. **Lizhi Zhang**: Project administration, Supervision, Writing – review & editing.

Declaration of Competing Interest

The authors declare that they have no known competing financial interests or personal relationships that could have appeared to influence the work reported in this paper.

Data Availability

Data will be made available on request.

Acknowledgments

This work was financially supported by the National Natural Science Foundation of China (Grant U22A20402, 21936003, 22076061, 22176068), the National Key Research and Development Program of China (2021YFA1201701), the Fundamental Research Funds for the Central Universities (CCNU22JC014), and the open fund from Shanghai Engineering Research Center of Solid Waste Treatment and Resource Recovery (2021GFZX007).

Appendix A. Supporting information

Supplementary data associated with this article can be found in the online version at doi:10.1016/j.apcatb.2023.122619.

References

[1] S. Cao, K. Wang, S. Zhou, Y. Wang, B. Liu, B. Cheng, Y. Li, Mechanism and effect of high-basicity chromium agent acting on Cr-wastewater-reuse system of leather industry, ACS Substain, Chem. Eng. 6 (2018) 3957–3963.
[2] S. Elabbas, L. Mandi, F. Berrekhis, M. Noelle Pons, J. Pierre Leclerc, N. Ouazzani, Removal of Cr(III) from chrome tanning wastewater by adsorption using two natural carbonaceous materials: eggshell and powdered marble, J. Environ. Manag. 166 (2016) 589–595.
[3] M. Owlad, M.K. Aroua, W.A.W. Daud, S. Baroutian, Removal of hexavalent chromium-contaminated water and wastewater: a review, Water Air Soil Poll. 200 (2009) 59–77.
[4] D. Wang, S. He, C. Shan, Y. Ye, H. Ma, X. Zhang, W. Zhang, B. Pan, Chromium speciation in tannery effluent after alkaline precipitation: Isolation and characterization, J. Hazard. Mater. 316 (2016) 169–177.
[5] J.P. Gustafsson, I. Persson, A.G. Oromieh, J.W.J. van Schaik, C. Sjostedt, D.B. Kleja, Chromium(III) complexation to natural organic matter: mechanisms and modeling, Environ. Sci. Technol. 48 (2014) 1753–1761.
[6] A.R. Walsh, J. O'Halloran, Chromium speciation in tannery effluent—II. Speciation in the effluent and in a receiving estuary, Water Res 30 (1996) 2401–2412.
[7] T.H. Madden, A.K. Datye, M. Fulton, M.R. Prairie, S.A. Majumdar, B.M. Stange, Oxidation of metal−EDTA complexes by TiO_2 photocatalysis, Environ. Sci. Technol. 31 (1997) 3475–3481.
[8] F. Fu, Q. Wang, B. Tang, Fenton and Fenton-like reaction followed by hydroxide precipitation in the removal of Ni(II) from NiEDTA wastewater: A comparative study, Chem. Eng. J. 155 (2009) 769–774.
[9] D. Jiraroj, F. Unob, A. Hagege, Degradation of Pb-EDTA complex by a H2O2/UV process, Water Res 40 (2006) 107–112.
[10] Y. Wang, Y. Liu, B. Wu, M. Rui, J. Liu, G. Lu, Comparison of toxicity induced by EDTA-Cu after UV/H_2O_2 and UV/persulfate treatment: Species-specific and technology-dependent toxicity, Chemosphere 240 (2020), 124943.
[11] Y. Ye, Z. Jiang, Z. Xu, X. Zhang, D. Wang, L. Lv, B. Pan, Efficient removal of Cr(III)-organic complexes from water using UV/Fe(III) system: Negligible Cr(VI) accumulation and mechanism, Water Res. 126 (2017) 172–178.
[12] Y. Ye, C. Shan, X. Zhang, H. Liu, D. Wang, L. Lv, B. Pan, Water decontamination from Cr(III)-organic complexes based on Pyrite/H2O2: performance, mechanism, and validation, Environ. Sci. Technol. 52 (2018) 10657–10664.
[13] B. Jiang, Q. Niu, C. Li, N. Oturan, M.A. Oturan, Outstanding performance of electro-Fenton process for efficient decontamination of Cr(III) complexes via alkaline precipitation with no accumulation of Cr(VI): Important roles of iron species, Appl. Catal. B: Environ. 272 (2020), 119002.
[14] Y. Yuan, W. Zhao, Z. Liu, C. Ling, C. Zhu, F. Liu, A. Li, Low-Fe(III) driven UV/Air process for enhanced recovery of heavy metals from EDTA complexed system, Water Res 171 (2020), 115375.
[15] F. Rezaei, D. Vione, Effect of pH on zero valent iron performance in heterogeneous fenton and fenton-like processes: a review, Molecules 23 (2018) 3127.
[16] Q. Li, Z. Jiang, J. Zheng, Y. Xie, Q. Liao, F. Zhao, Z. Yang, Z. Lin, M. Si, W. Yang, Interaction of pyrite with zerovalent iron with superior reductive ability via Fe(ii) regeneration, Environ. Sci.: Nano 9 (2022) 2713–2725.
[17] W. Yang, Q. Li, Y. He, D. Xi, C. Arinzechi, X.M. Zhang, Q. Liao, Z.H. Yang, M.Y. Si, Synergistic Cr(VI) reduction and adsorption of Cu(II), Co(II) and Ni(II) by zerovalent iron-loaded hydroxyapatite, Chemosphere 313 (2023), 137428.
[18] W. Yang, D. Xi, C. Li, Z. Yang, Z. Lin, M. Si, In-situ synthesized iron-based bimetal promotes efficient removal of Cr(VI) by zero-valent iron-loaded hydroxyapatite, J. Hazard. Mater. 420 (2021), 126540.
[19] F. Fu, L. Xie, B. Tang, Q. Wang, S. Jiang, Application of a novel strategy-advanced fenton-chemical precipitation to the treatment of strong stability chelated heavy metal containing wastewater, Chem. Eng. J. 189 (2012) 283–287.
[20] Z. Ai, Z. Gao, L. Zhang, W. He, J. Yin, Core-shell structure dependent reactivity of Fe@Fe_2O_3 nanowires on aerobic degradation of 4-chlorophenol, Environ. Sci. Technol. 47 (2013) 5344–5352.
[21] Y. Mu, Z. Ai, L. Zhang, Phosphate shifted oxygen reduction pathway on Fe@Fe_2O_3 core-shell nanowires for enhanced reactive oxygen species generation and aerobic 4-chlorophenol degradation, Environ. Sci. Technol. 51 (2017) 8101–8109.
[22] Y. Mu, F. Jia, Z. Ai, L. Zhang, Iron oxide shell mediated environmental remediation properties of nano zero-valent iron, Environ. Sci. Nano 4 (2017) 27–45.
[23] C. Lee, Oxidation of organic contaminants in water by iron-induced oxygen activation: a short review, Environ. Eng. Res. 20 (2015) 205–211.
[24] M. Liao, X. Wang, S. Cao, M. Li, X. Peng, L. Zhang, Oxalate modification dramatically promoted Cr(VI) removal with zero-valent iron, ACS ES&T Water 1 (2021) 2109–2118.
[25] Y. Hu, G. Zhan, X. Peng, X. Liu, Z. Ai, F. Jia, S. Cao, F. Quan, W. Shen, L. Zhang, Enhanced Cr(VI) removal of zero-valent iron with high proton conductive FeC_2O_4 center dot 2H(2)O shell, Chem. Eng. J. 389 (2020).
[26] Y. Hu, X. Peng, Z. Ai, F. Jia, L. Zhang, Liquid nitrogen activation of zero-valent iron and its enhanced Cr(VI) removal performance, Environ. Sci. Technol. 53 (2019) 8333–8341.
[27] N. Chen, Y. Huang, X. Hou, Z. Ai, L. Zhang, Photochemistry of hydrochar: reactive oxygen species generation and sulfadimidine degradation, Environ. Sci. Technol. 51 (2017) 11278–11287.
[28] B. Nowack, F.G. Kari, S.U. Hilger, L. Sigg, Determination of dissolved and adsorbed EDTA species in water and sediments by HPLC, Anal. Chem. 68 (1996) 561–566.
[29] Z. Xu, G.D. Gao, B.C. Pan, W.M. Zhang, L. Lv, A new combined process for efficient removal of Cu(II) organic complexes from wastewater: Fe(III) displacement/UV degradation/alkaline precipitation, Water Res 87 (2015) 378–384.
[30] F. Fu, B. Tang, Q. Wang, J. Liu, Degradation of Ni-EDTA complex by Fenton reaction and ultrasonic treatment for the removal of Ni^{2+} ions, Environ. Chem. Lett. 8 (2010) 317–322.
[31] L. Wang, M. Cao, Z. Ai, L. Zhang, Dramatically enhanced aerobic atrazine degradation with Fe@Fe_2O_3 core-shell nanowires by tetrapolyphosphate, Environ. Sci. Technol. 48 (2014) 3354–3362.

[32] Z. Yang, J. Qian, A. Yu, B. Pan, Singlet oxygen mediated iron-based Fenton-like catalysis under nanoconfinement, Proc. Natl. Acad. Sci. USA 116 (2019) 6659–6664.
[33] Y. Nosaka, A.Y. Nosaka, Generation and detection of reactive oxygen species in photocatalysis, Chem. Rev. 117 (2017) 11302–11336.
[34] H. Dong, Y. Li, S. Wang, W. Liu, G. Zhou, Y. Xie, X. Guan, Both Fe(IV) and radicals are active oxidants in the Fe(II)/Peroxydisulfate process solution, Environ. Sci. Technol. Let. 7 (2020) 219–224.
[35] A.D. Bokare, W. Choi, Singlet-oxygen generation in alkaline periodate solution, Environ. Sci. Technol. Let. 49 (2015) 14392–14400.
[36] J.M. Allen, C.J. Gossett, S.K. Allen, Photochemical formation of singlet molecular oxygen in illuminated aqueous solutions of several commercially available sunscreen active ingredients, Chem. Res. Toxicol. 9 (1996) 605–609.
[37] E.M. Cuerda-Correa, M.F. Alexandre-Franco, C. Fernandez-Gonzalez, Advanced oxidation processes for the removal of antibiotics from water, Overv. Water 12 (2020).
[38] C. Pierlot, V. Nardello-Rataj, J.-M. Aubry, Simultaneous determination of the chemical (k(r)) and the physical (k(q)) quenching rate constants of singlet oxygen in aqueous solution by the chemiluminescence-quenching method(dagger), Photochem. Photobiol. 97 (2021) 1343–1352.
[39] C. Chen, P. Liu, Y. Li, H. Tian, Y. Zhang, X. Zheng, R. Liu, M. Zhao, X. Huang, Electro-peroxone enables efficient Cr removal and recovery from Cr(III) complexes and inhibits intermediate Cr(VI) generation in wastewater: Performance and mechanism, Water Res. 218 (2022), 118502.
[40] S. Liang, X. Hu, H. Xu, Z. Lei, C. Wei, C. Feng, Mechanistic insight into the reaction pathway of peroxomonosulfate-initiated decomplexation of EDTA-Ni-II under alkaline conditions: Formation of high-valent Ni intermediate, Appl. Catal. B: Environ. 296 (2021), 120375.